Climate Dynamics manuscript No.
(will be inserted by the editor)

Global Warming and 21st Century Drying

Benjamin I Cook · Jason E Smerdon · Richard Seager · Sloan Coats

Received: date / Accepted: date

Abstract Global warming is expected to increase the frequency and intensity of droughts in the 21st century, but the relative contributions from changes in moisture supply (precipitation) versus evaporative demand (potential evapotranspiration; PET) have not been comprehensively assessed. Using output from a suite of general circulation model (GCM) simulations from version 5 of the Coupled Model Intercomparison Project, projected 21st-century drying and wetting trends are investigated using two offline indices of surface moisture balance: the Palmer Drought Severity Index (PDSI) and the Standardized Precipitation Evapotranspiration Index (SPEI). PDSI and SPEI projections using precipitation and Penman-Monteith based PET changes from the GCMs generally agree, showing robust cross-model drying in western North America, Central America, the Mediterranean, southern Africa, and the Amazon and robust wetting occurring in the Northern Hemisphere high latitudes and east Africa (PDSI only). The SPEI is more sensitive to PET changes than the PDSI, especially in arid regions such as the Sahara and Middle East. Regional drying and wetting patterns largely mirror the spatially heterogeneous response of precipitation in the models, although drying in the PDSI and SPEI calculations extends beyond the regions of reduced precipitation. This expansion of drying areas is attributed to globally widespread increases in PET, caused by increases in surface net radiation and the vapor pressure deficit. Increased PET not only intensifies drying in areas where precipitation is already reduced, it also drives areas into drought that would otherwise experience little

Benjamin I Cook
NASA Goddard Institute for Space Studies
2880 Broadway, New York, NY 10025
Tel.: (212) 678-5669
E-mail: benjamin.i.cook@nasa.gov

Jason E Smerdon
Lamont-Doherty Earth Observatory, 61 Route 9W, Palisades, NY, 10964

Richard Seager
Lamont-Doherty Earth Observatory, 61 Route 9W, Palisades, NY, 10964

Sloan Coats
Lamont-Doherty Earth Observatory, 61 Route 9W, Palisades, NY, 10964

drying or even wetting from precipitation trends alone. This PET amplification effect is largest in the Northern Hemisphere mid-latitudes, and is especially pronounced in western North America, Europe, and southeast China. Compared to PDSI projections using precipitation changes only, the projections incorporating both precipitation and PET changes increase the percentage of global land area projected to experience at least moderate drying (PDSI standard deviation of ≤ -1) by the end of the 21st-century from 12% to 30%. PET induced moderate drying is even more severe in the SPEI projections (SPEI standard deviation of ≤ -1; 11% to 44%), although this is likely less meaningful because much of the PET induced drying in the SPEI occurs in the aforementioned arid regions. Integrated accounting of both the supply and demand sides of the surface moisture balance is therefore critical for characterizing the full range of projected drought risks tied to increasing greenhouse gases and associated warming of the climate system.

1 Introduction

Extreme climate and weather events have caused significant disruptions to modern and past societies (Coumou and Rahmstorf, 2012; Ross and Lott, 2003; Lubchenco and Karl, 2012), and there is concern that anthropogenic climate change will increase the occurrence, magnitude, or impact of these events in the future (e.g., Meehl et al, 2000; Rahmstorf and Coumou, 2011). Drought is one such extreme phenomenon, and is of particular interest because of it's often long-term impacts on critical water resources, agricultural production, and economic activity (e.g., Li et al, 2011; Ding et al, 2011; Ross and Lott, 2003). Focus on drought vulnerabilities has increased due to a series of recent and severe droughts in regions as diverse as the United States (Hoerling et al, 2012a, 2013; Karl et al, 2012), east Africa (Lyon and DeWitt, 2012), Australia (McGrath et al, 2012), and the Sahel (Giannini et al, 2003). Recent work further suggests that global aridity has increased in step with observed warming trends, and that this drying will worsen for many regions as global temperatures continue to rise with increasing anthropogenic greenhouse gas emissions (Burke et al, 2006; Dai, 2013; Sheffield and Wood, 2008).

There are significant uncertainties, however, in recent and projected future drought trends, especially regarding the extent to which these trends will be forced by changes in precipitation versus evaporative demand (Hoerling et al, 2012b; Sheffield et al, 2012). Drought is generally defined as a deficit in soil moisture (agricultural) or streamflow (hydrologic); as such, it can be caused by declines in precipitation, increases in evapotranspiration, or a combination of the two. In the global mean, both precipitation and evapotranspiration are expected to increase with warming, a consequence of an intensified hydrologic cycle in a warmer world (Allen and Ingram, 2002; Huntington, 2006). Regional changes in precipitation and evapotranspiration, and the dynamics that drive such changes, are nevertheless more uncertain, despite the fact that these changes are perhaps of greatest relevance to on-the-ground stakeholders.

Precipitation projections in general circulation models (GCMs) have large uncertainties compared to other model variables, such as temperature (e.g., Knutti and Sedlacek, 2013). The most confident estimates indicate that precipitation will increase in mesic areas (e.g., the wet tropics, the mid- to high latitudes of the

Northern Hemisphere, etc) and decrease in semi-arid regions (e.g., the subtropics). This is generally referred to as the 'rich-get-richer/poor-get-poorer' mechanism, and is attributed to thermodynamic (warming and moistening of the atmosphere) and dynamic (circulation) processes (Chou et al, 2009, 2013; Held and Soden, 2006; Neelin et al, 2003; Seager et al, 2010).

Evapotranspiration includes both the physical (evaporation) and biological (transpiration) fluxes of moisture from the surface to the atmosphere and can be viewed in terms of actual evapotranspiration (latent heat flux) or evaporative demand (potential evapotranspiration; PET). PET is expected to increase in the future (Scheff and Frierson, 2013), forced by increases in both total energy availability at the surface (surface net radiation) and the vapor pressure deficit (the difference between saturation and actual vapor pressure; VPD). Increased radiative forcing from anthropogenic greenhouse gases (GHG) will increase surface net radiation in most areas by inhibiting longwave cooling, while GHG-induced warming of the atmosphere will increase the VPD. Importantly, VPD increases with warming, even at constant relative humidity (e.g., Anderson, 1936). Actual evapotranspiration is expected to increase less than PET in areas where latent heat fluxes are, or will become, limited by moisture supply. Indeed, declines in global actual evapotranspiration have been documented over the last two decades (Jung et al, 2010), attributed primarily to soil moisture drying in the Southern Hemisphere.

The idea that increased evaporative demand in a warmer world will enhance drought is not new (e.g., Dai, 2011b), but it is important to understand where precipitation or evaporation changes will be dominant individual drivers of drought and where they will work in concert to intensify drought. To date, however, little has been done to quantify and explicitly separate the relative contribution of changes in precipitation versus evaporative demand to the magnitude and extent of global warming-induced drying. To address this question, we use output from a suite of 20$^{\text{th}}$ and 21$^{\text{st}}$-century GCM simulations, available through the Coupled Model Intercomparison Project version 5 (CMIP5, Taylor et al, 2012), to calculate two offline indices of surface moisture balance: the Palmer Drought Severity Index (PDSI; Palmer, 1965) and the Standardized Precipitation Evapotranspiration Index (SPEI; Vicente-Serrano et al, 2009). Both indices provide ideal and flexible estimations of surface moisture balance, allowing us to vary inputs such as model precipitation, temperature, and surface energy availability in order to separate and quantify the influence of specific variables on future drought projections. Our analysis thus addresses three questions: 1) What are the relative contributions of changes in precipitation and evaporative demand to global and regional drying patterns?, 2) Where do the combined effects of changes in precipitation and evaporative demand enhance drying?, and 3) In which regions, if any, are increases in evaporative demand sufficient to shift the climate towards drought when precipitation changes would otherwise force wetter conditions?

2 Data and Methods

2.1 CMIP5 Model Output

We use GCM output available from the CMIP5 archive, the suite of model experiments organized and contributed from various modeling centers in support of the Fifth Assessment Report (AR5) of the Intergovernmental Panel on Climate Change (IPCC). Output from the historical and RCP8.5 model scenarios is used. The historical experiments are run for the years 1850–2005 and are forced with observations of transient climate forcings over the last 150 years (e.g., solar variability, land use change, GHG concentrations, etc). These experiments are initialized in 1850 using output from long, unforced control runs with fixed pre-industrial climate forcings. The RCP8.5 scenario (2006–2099) is one of a suite of future GHG forcing scenarios; RCP8.5 is designed so that the top of the atmosphere radiative imbalance will equal approximately +8.5 W m^{-2} by the end of the 21^{st}-century, relative to pre-industrial conditions. The RCP8.5 scenario runs are initialized using the end of the historical runs. Our analysis is restricted to those models (Table 1) with continuous ensemble members spanning the historical through RCP8.5 time periods.

2.2 Drought Indices

For our analysis, we are interested in long-term (decadal to centennial) trends and changes in moisture availability, rather than shorter-term (month to month) drought events. For this reason, our analysis uses two drought indices that integrate over longer timescales: the PDSI and 12-month SPEI. Understanding the causes, inception, and termination of discrete (and often short and intense) drought events (e.g., Hoerling et al, 2012a, 2013) is an important scientific goal. Our focus, however, is on the longer-term drying and wetting responses to GHG warming, the hydroclimatic baseline within which seasonal or annual events will occur in the future.

Simulated soil moisture within the GCMs is not easily separated into contributions from precipitation or PET, making it difficult to identify the extent to which soil moisture trends in the models are driven by changes in supply and/or demand. Moreover, each GCM employs soil models that vary widely in their sophistication (e.g., soil depth, number of layers, etc), tunings, and parameterizations (e.g., soil texture, rooting depths, vegetation types, etc), complicating the meaningful comparison of soil moisture and drought responses across GCMs. PDSI and SPEI provide a flexible framework that allows GCM output to be modified (e.g., detrended) as a means of isolating drought contributions from specific changes, such as trends in precipitation or net radiation. A common offline metric, such as PDSI or SPEI, also provides a standard comparison of soil moisture balance, thus controlling for differences in soil models across the ensemble of CMIP5 GCMs.

The PDSI (Palmer, 1965) is a normalized index of drought using a simplified soil moisture balance model calculated from inputs of precipitation and losses from evapotranspiration. PDSI is locally normalized, with negative values indicating drier than normal conditions (droughts) and positive values indicating wetter than normal conditions (pluvials), relative to a baseline calibration period for a given location. PDSI has persistence on the order of 12–18 months (Guttman, 1998; Vicente-Serrano et al, 2010), integrating moisture gains and losses throughout the calendar year, and providing a useful metric to describe longer term trends and variability in hydroclimate. PDSI has been widely used as a metric to quantify drought using climate model simulations (e.g., Bonsal et al, 2013; Burke and Brown, 2008; Coats et al, 2013; Cook et al, 2010, 2013; Dai, 2011b, 2013; Rosenzweig and Hillel, 1993; Seager et al, 2008; Taylor et al, 2013).

Because recent work has suggested that PDSI may be intrinsically too sensitive to changes in PET (e.g., Burke, 2011; Seneviratne, 2012), we repeat our analysis using an alternative drought index, the SPEI. Like PDSI, SPEI (Vicente-Serrano et al, 2009) is a normalized index of drought, developed from the original Standardized Precipitation Index (SPI, McKee et al, 1993). Whereas the SPI is based on normalized accumulations of precipitation surpluses and deficits over some user-defined interval (typically 1, 3, or 12 months), SPEI uses accumulations of precipitation minus PET. Therefore, SPEI includes in it's accounting both supply and demand changes in moisture variability, and can be interpreted similarly to PDSI (i.e., positive values of SPEI indicate wetter than average conditions, negative values indicate drier than average conditions). Unlike PDSI, SPEI does not include an explicit soil moisture balance accounting, and only uses information on precipitation minus PET to curve fit and calculate standardized departures of moisture availability. Similar to PDSI, SPEI has been used previously in GCM based climate projections (e.g., Barrera-Escoda et al, 2013; Hernandez and Uddameri, 2013).

Recent studies have highlighted some deficiencies regarding the Thornthwaite (Thornthwaite, 1948) temperature-based method often used for estimating PET in PDSI and SPEI calculations (Dai, 2011b; Hoerling et al, 2012b; Sheffield et al, 2012; Vicente-Serrano et al, 2009). The Thornthwaite method of estimating PET has the advantage of only requiring temperature data, and so has been widely used for PET calculations, especially over the historical period. Because Thornthwaite is largely a linear rescaling of temperature to PET, it significantly overestimates PET and drying when temperatures increase significantly beyond the mean of the baseline calibration period. This has led to several studies (e.g., Hoerling et al, 2012b; Sheffield et al, 2012) concluding that Thornthwaite based estimates of PET are inappropriate for use in global warming projections of drought.

Recently, there has been support for the use of the Penman-Monteith method (Penman, 1948; Xu and Singh, 2002) as an alternative to Thornthwaite for calculating PET for drought projections (Dai, 2011a, 2013; Hoerling et al, 2012b; van der Schrier et al, 2013; Sheffield et al, 2012). Penman-Monteith is based on surface moisture and energy balance considerations (Xu and Singh, 2002), and a commonly used version is the formulation provided by the Food and Agricultural Organization (FAO) of the United Nations (Allen et al, 1998):

$$PET = \frac{0.408\Delta(R_n - G) + \gamma\frac{900}{T_a+273}u_2(e_s - e_a)}{\Delta + \gamma(1 + 0.34u_2)} \quad (1)$$

where PET is potential evapotranspiration (mm day^{-1}), Δ is the slope of the vapor pressure curve (kPa $^{\circ}$C^{-1}), R_n is surface net radiation (MJ m^{-2} day^{-1}), G is the soil heat flux density (MJ m^{-2} day^{-1}), γ is the psychometric constant (kPa $^{\circ}$C^{-1}), T_a is the air temperature at 2-meters ($^{\circ}$C), u_2 is the wind speed at 2-meters (m s^{-1}), e_s is the saturation vapor pressure (kPa), and e_a is the actual vapor pressure (kPa). The VPD is defined as $e_s - e_a$. Penman-Monteith based PDSI has been used, with good success, to track both observational changes in drought and changes in future drought (Dai, 2013; van der Schrier et al, 2013), and is not subject to unrealistic temperature scaling outside of the normalization interval as demonstrated for the Thornthwaite-based PDSI (Hoerling et al, 2012b; Sheffield et al, 2012). We therefore use Penman-Monteith PET in all of our PDSI and SPEI calculations for two principal reasons. First, our motivation is to analyze 21^{st}-century projections of hydroclimate relative to a 20^{th}-century baseline, the former of which involves temperature increases well outside the climatology of the latter. Second, the more detailed and realistic formulation of PET in the Penman-Monteith formalism allows us to separate specific variable influences on PET and therefore characterize PET-influenced drying in terms of the net radiation and VPD changes that cause them.

2.3 Analyses

In the PDSI soil moisture calculation, we set the soil moisture capacities for the top and bottom layers to the standard values of 25.4 mm (1 in.) and 127 mm (5 in.). We use the 1931–1990 period from the historical runs as our baseline calibration period for the normalization, the same time interval used by the National Oceanographic and Atmospheric Administration for normalization of their PDSI calculations. In order to maximize comparability with the PDSI, we use a 12-month interval for accumulating precipitation minus PET anomalies in our SPEI calculations, and also use the same standardization interval (1931–1990). PDSI and SPEI are calculated separately for each individual ensemble member at the native resolution of the model.

Diagnostics used from each GCM are monthly values of precipitation, 2-meter air temperature, surface pressure and 2-meter surface specific humidity (used to calculate vapor pressure), and surface net radiation. Ground heat flux and surface wind speed diagnostics were more difficult to obtain from these models. Relative to changes in energy availability and the VPD, Penman-Monteith PET is relatively insensitive to wind speed (e.g., Scheff and Frierson, 2013); we therefore set $u_2 = 1$. Additionally, ground heat fluxes (G) are usually only a small fraction of the total surface energy budget, about 10–15% (Betts et al, 1996; Sellers et al, 1997). Tests in which we alternately set G to 0 or 15% of R_n indicated that the PDSI calculation is largely insensitive to this parameter. For the analyses presented herein, we therefore set $G = 0$.

For each continuous historical+RCP8.5 ensemble member, we calculate three different versions of PDSI and SPEI (Table 2) from 1900–2099 that serve as the basis for the majority of our analyses. PDSI-ALL and SPEI-ALL references the full calculation, incorporating changes in both precipitation and PET by using the original values of all the model variables, including their trends, from 1900 to 2099. In PDSI-PRE and SPEI-PRE, we isolate the impact of precipitation by detrending the temperature, vapor pressure, and net radiation variables from 2000–2099, and setting the 21^{st}-century mean to be equal to the mean of the last two decades of the 20^{th} century (thus retaining the variability but removing any trend from 2000–2099). In PDSI-PET and SPEI-PET, we isolate the impact of changes in evaporative demand by detrending the precipitation using an identical procedure, and retaining the transient changes in temperature, surface net radiation, and vapor pressure. We also conduct additional PDSI and SPEI calculations to examine specific impacts of changes in VPD only (by detrending R_n and precipitation) and net radiation only (by detrending T, vapor pressure, and precipitation). For cross-model comparisons of PDSI, SPEI, and model diagnostics, all models are spatially interpolated to a common 2^ox2^o spatial grid. For models with multiple ensemble members, the intra-model ensemble average is calculated before the multi-model ensemble average to maintain equal weighting across the 15 models. Changes in model climate variables are calculated as 2080–2099 minus 1931–1990, the same modern baseline period for the PDSI and SPEI normalizations.

To demonstrate the ability of the PDSI and SPEI to represent changes in surface moisture balance, we calculated Pearson's correlation coefficients between annual average PDSI and SPEI and annual average standardized soil moisture anomalies for each grid cell for two of the models: CanESM2 and CCSM4 (Figure 1) (level-by-level soil moisture fields are not available from all models or ensemble members in the employed suite of CMIP5 models). Soil moisture anomalies are based on the approximate top 30 centimeters of the soil column. The correlation maps show strongly positive correlations between soil moisture and PDSI and SPEI, with some isolated areas of weaker correlation. For CanESM2, 94% of land grid cells (excluding Antarctica) have positive and significant ($p \leq 0.05$) correlations between PDSI and soil moisture, with similar results for SPEI (91%). Results are similar for CCSM4: 96% of grid cells have significant and positive correlations between soil moisture and PDSI or SPEI. Differences between the soil moisture and PDSI/SPEI fields likely arise through some of the aforementioned structural differences between the GCM land surface models and the PDSI/SPEI calculations. The strong and highly positive correlations nevertheless indicate that PDSI and SPEI represent well the variability in modeled surface moisture balance.

The efficacy of using precipitation-only (PDSI-PRE and SPEI-PRE) or PET-only (PDSI-PET and SPEI-PET) based indices to separate the influences of changing precipitation and evaporative demand on future drought depends on these quantities being approximately independent in their contribution to the full hydroclimate response (PDSI-ALL and SPEI-ALL). While they are not likely to be completely independent, because changes in precipitation will, for many regions, affect surface radiation, temperature, and other variables, we require that to first order they sum linearly for our interpretations of precipitation and evaporative demand contributions to drought. We compare PDSI-ALL to the sum of PDSI-PRE and PDSI-PET (PDSI-SUM; Figure 2) and SPEI-ALL to the sum of SPEI-PRE and SPEI-PET (SPEI-SUM; Figure 3) for each grid cell, averaged over 2080–2099. The 1:1 line, indicating a perfect match between PDSI-ALL and PDSI-SUM or SPEI-ALL and SPEI-SUM, is plotted as the dashed black lines in all the panels. For both PDSI and SPEI, the 'SUM' and 'ALL' values for each model track each other closely and scatter evenly around the 1:1 line. This close match indicates that our interpretations of the 'PRE' and 'PET' calculations as separate and additive constituents of regional drought trends are appropriate for the models and range of climate changes considered herein.

3 Results

3.1 Model Climate Response

The forced response in surface climate from our chosen subset of CMIP5 models (Figure 4) is consistent with previous analyses of the CMIP5 climate projections (e.g., Knutti and Sedlacek, 2013). Cross-hatching in Figure 4 indicates areas where at least 12 of the 15 models (80%) agree with the sign of the change in the multi-model mean. Surface net radiation increases primarily through the inhibition of longwave cooling by increased anthropogenic GHG concentrations (Figure 4a). Land surface temperatures increase everywhere (Figure 4b), with amplified warming in the Northern Hemisphere high latitudes. Precipitation responses (Figure 4c) are spatially heterogenous, with some regions showing drying (e.g., southwest North America, the Mediterranean, southern Africa) and others wetting (e.g., the high latitudes in the Northern Hemisphere), as per the rich-get-richer/poor-get-poorer mechanism discussed previously. Consistent with expectations, precipitation changes show much less consistency across models than the changes in surface net radiation or surface temperature. The VPD increases across all land areas (Figure 4d), primarily as a consequence of the globally widespread warming, with the largest increases occurring in regions that are projected to warm and dry (e.g., South America, southern Africa).

The models also show regional changes in summer season (JJA in the Northern Hemisphere; DJF in the Southern Hemisphere) actual evapotranspiration (latent heat fluxes; Figure 4e) and the ratio of latent heating to the sum of sensible plus latent heating (evaporative fraction or EF, Figure 4f). Evapotranspiration (Figure 4e) increases in much of the wet tropics and the Northern Hemisphere high latitudes, where evaporative demand is enhanced (via increased VPD and surface net radiation) and precipitation generally increases. These are areas where evaporation is primarily energy (rather than moisture) limited and where evaporation continues to be energy limited in the future. In the sub-tropics, where evapotranspiration is primarily controlled by surface moisture availability, evapotranspiration decreases as surface moisture is unable to satisfy the increased atmospheric demand.

Changes in EF (Figure 4f) provide a diagnostic for changing moisture versus energy limitations to evaptranspiration in the future. Areas with declining EF are regions where evapotranspiration rates are increasingly moisture limited. This includes much of the sub-tropics, where evapotranspiration is declining, but also areas of the mid-latitudes where evapotranspiration is projected to increase (e.g., Central Plains of North America and Europe). The fact that EF decreases in areas of both increased and decreased evapotranspiration is suggestive of an overall decline in surface and soil moisture availability in these regions. Increases in EF are confined primarily to areas where precipitation is increasing and evapotranspiration is limited by energy demand, such as the high latitudes of the Northern Hemisphere.

3.2 Model PDSI and SPEI Response

Annual average PDSI and SPEI values for each model and for all calculations (ALL, PRE, PET) at the end of the 21st century (2080–2099) are shown in Figures 5–10. Multi-model means for these same quantities are in Figure 11; cross hatching indicates areas where the multi-model mean PDSI anomalies exceed -1 or $+1$ or where multi-model mean SPEI values exceed -0.5 or $+0.5$ (PDSI and SPEI are qualitatively similar, but use different scalings), and where at least 12 of the 15 models also exceed these thresholds. The PDSI-ALL and SPEI-ALL projections (Figure 11a,b) indicate substantial and robust drying over much of North America, the Amazon Basin, southern Africa, the Mediterranean, Europe, southeast China, and parts of Australia. Wetting occurs primarily at high latitudes in the Northern Hemisphere and east Africa, although these changes are more consistent across models (cross-hatching) in the PDSI calculations than SPEI. Areas of drying in PDSI-ALL and SPEI-ALL generally overlap regions with declining EF (Figure 4f), further supporting the use of PDSI and SPEI as measures of surface moisture availability. When precipitation effects are isolated (PDSI-PRE and SPEI-PRE, Figure 11c,d), the resulting pattern closely mirrors the changes in precipitation (Figure 4c), with substantially reduced drying in many regions relative to PDSI-ALL and SPEI-ALL, especially in the mid-latitudes. These results clearly indicate that, while the global pattern of hydroclimatic change is organized around the centers of suppressed and enhanced precipitation, precipitation changes alone cannot explain the full magnitude or spatial extent of drying documented by the complete PDSI and SPEI accountings, or seen in the multi-model mean EF changes. Maps of PDSI-PET and SPEI-PET (Figure 11e,f) demonstrate that this additional drying is the result of increased PET. Changes in PDSI-PET and SPEI-PET show nearly uniform drying of all land areas, an expected consequence of the more widespread and uniform nature of changes in surface net radiation (Figure 4a) and VPD (Figure 4d) compared to precipitation (Figure 4c). When surface net radiation and VPD contributions to the drying are individually separated (Figure 12), it is clear that the relative impact of increases in the VPD is substantially larger than the effect of surface net radiation, especially in the Northern Hemisphere. The influence of net radiation versus VPD changes on PET is discussed in more detail elsewhere (Scheff and Frierson, 2013).

While PDSI and SPEI are qualitatively similar, they use different scalings and require some degree of renormalization to be directly comparable. In order to calculate the spatial extent of the drying in the various PDSI and SPEI calculations, we renormalized the annual average PDSI and SPEI values to have a mean of zero and inter-annual standard deviation of one over the original standardization period (1931–1990). These Z-indices are directly comparable between PDSI and SPEI, and are used to calculate the fraction of land area (excluding Antarctica) with negative PDSI and SPEI anomalies exceeding 1, 2, or 3 standard deviations at the end of the 21^{st} century (Figure 13). Using a PDSI threshold of one standard deviation ($Z \leq -1$, Figure 13a), for example, precipitation changes alone (PDSI-PRE) cause drying on only about 12% of the global land area in the multi-model mean. Considering only increases in PET (PDSI-PET), however, leads to an equivalent magnitude of drying on nearly 44% of the global land area, an expected result given the much wider and monotonic pattern of PET increases in the models. For the fully simulated hydroclimate response (PDSI-ALL), the percent of land area exceeding the $Z \leq -1$ threshold is between these two estimates, at about 30%. This reflects the fact that, depending on the region, combined PET and precipitation effects will either act to reinforce the drying ($+PET$,$-precipitation$) or act in opposition to each other, resulting in either wetting ($+precipitation >> +PET$), drying ($+PET >> +precipitation$), or little change ($+PET \approx +precipitation$). Results are similar for the SPEI Z-indices (Figure 13b), but SPEI indicates much more widespread drying from the increases in PET, reflective of what is a greater sensitivity of the SPEI to PET changes than PDSI, especially in arid regions with little rainfall, such as the Sahara and Middle East (Figures 11 and 12). PDSI is constrained by a soil moisture accounting that depends on it's internally calculated actual evapotranspiration, using the provided Penman-Monteith PET as an initial starting value (Dai, 2011a). This constraint is especially important in more arid regions where evapotranspiration rates are limited primarily by soil moisture availability, rather than atmospheric demand reflected in the PET. SPEI, by contrast, has no such actual evapotranspiration or soil moisture limitation built in, and will continually respond to changes in PET, even when drying reaches the point that actual evapotranspiration should be supply limited. In this way, PDSI may offer some advantages over SPEI (Dai, 2011a). This difference between the PDSI and SPEI accounting is reflected in the overall higher correlations between PDSI and model soil moisture (Figure 1). Unfortunately, masking of these arid regions in the models is difficult do in such a way that would allow easy cross-model comparisons: because of model precipitation biases, these arid regions vary across the GCMs in terms of their size and location.

Amplification of the drying by increases in PET is further demonstrated in the zonal average PDSI and SPEI calculated from the multi-model mean (Figure 14). In PDSI-PRE and SPEI-PRE (green lines), nearly the entire Northern Hemisphere in the zonal mean gets wetter, with the greatest increase occurring in the high latitudes where precipitation increases are largest. PDSI-PRE and SPEI-PRE changes in the mid-latitudes (30°N–50°N) are near neutral or slightly wetter; in these latitude bands, precipitation increases in some regions are largely counteracted by declines in other areas along this zonal band (Figure 4c). Increases in PET, reflected in PDSI-PET and SPEI-PET (red lines), result in drying across all latitudes. When both PET and precipitation are considered (PDSI-ALL and SPEI-PET, brown lines), the net result is such that PET increases counter a substantial fraction of the precipitation-driven wetting in the high northern latitudes and actually push the mid-latitudes (30°N–50°N) into a drier mean state (PDSI<0 and SPEI<0).

Four regions where the PET effects are especially pronounced are the Central Plains of North America (105°W–90°W, 32°N–50°N; Figures 15a,16a), southeast China (102°E–123°E, 22°N–30°N; Figures 15b,16b), the European-Mediterranean region (20°W–50°E, 28°N–60°N; Figures 15c,16c), and the Amazon (70°W–45°W, 20°S–5°N; Figures 15d,16d). China and the North American Central Plains are especially notable because, without the effect of increased PET, these regions would be expected to stay near neutral (China, multi-model mean PDSI-PRE$=+0.11$ and SPEI-PRE$=+0.12$), or even get wetter (North American Central Plains, multi-model mean PDSI-PRE$=+0.63$ and SPEI-PRE$=+0.25$). Instead, both regions dry substantially in PDSI-ALL and SPEI-ALL, shifting to a mean values of PDSI$=-1.85$ and SPEI$=-0.90$ over the North American Central Plains and PDSI$=-1.51$ and SPEI$=-0.67$ over China. In other regions, PET changes act to not only expand the spatial footprint of the regional drying, but also to amplify the changes that do occur because of reduced precipitation. In the European-Mediterranean region, PET effects intensify and expand the drying northward from the Mediterranean, shifting the regional average PDSI from -0.50 (PDSI-PRE) to −2.53 (PDSI-ALL), and SPEI from −0.17 (SPEI-PRE) to −2.00 (SPEI-ALL). Similar intensification also happens in the Amazon, where precipitation effects result in a regional average drying (PDSI-PRE= −1.40, SPEI-PRE= −0.41), with the added effect of increased PET causing further drying in the region (PDSI-ALL=−3.25, SPEI-ALL=−1.33).

4 Discussion

Developing and refining projections of hydroclimate, drought, and water resources for the 21st century is an active area of research (e.g., Barnett and Pierce, 2009; Dai, 2013; Seager et al, 2013). Toward this end, significant advances have already been made in key areas, especially in our understanding of regional and seasonal precipitation responses to warming (Chou et al, 2009, 2013; Held and Soden, 2006; Neelin et al, 2003; Seager et al, 2010). Precipitation, however, does not represent the only control on ecologically and socially relevant water resources, such as streamflow, reservoir storage, and soil moisture. Evaporative demand from the atmosphere, driven by air temperature, humidity, and energy availability, can also play a critical role. It is generally accepted that a warmer world will increase evaporative demand and drying independent of precipitation changes (Dai, 2011b). To date, however, few efforts have been made to explicitly separate the relative contributions to future drought trends from changes in supply (precipitation) versus demand (PET).

Using the latest suite of state-of-the-art climate model projections and two indices of surface moisture balance (PDSI and SPEI), we find that robust regional changes in hydroclimate are, to first order, organized around regional changes in precipitation. Increases in precipitation cause wetting in the high northern latitudes and east Africa, and precipitation declines lead to drying in the sub-tropics and Amazon. In areas where declines in precipitation already push the climate towards drought (e.g., Central America, the Amazon, southern Africa, the Mediterranean, etc), increased PET amplifies the precipitation induced drying. Critically, PET also plays a major role in enhancing drying in the midlatitudes and along the margins of the sub-tropics, where precipitation changes are small or even positive. Globally, increased PET nearly triples the fractional land area that will experience drying exceeding one standard deviation of the PDSI index (Figure 13) by the end of the 21st century, from 12% (precipitation effects only, PDSI-PRE) to 30% (precipitation+PET effects, PDSI-ALL). In certain regions (e.g., western North America, Europe, and southeast China), PET is in fact the sole or primary driver shifting these areas into drought. Areas dominated by the Asian monsoon (India, Indochina, etc) are some of the few places where there is little change in mean hydroclimate. In these regions, gains in moisture from increased annual and monsoon precipitation (Lee and Wang, 2012; Seo et al, 2013) are large enough to compensate for any increases in PET.

Both PDSI and SPEI provide useful metrics of surface moisture balance as it relates to both supply and demand considerations. One factor neglected by these indices as formulated herein, however, is the potential effect of enhanced carbon dioxide concentrations in the atmosphere ([CO2]), which are expected to have a direct physiological effect on plants by reducing stomatal and canopy conductance, increasing the water use efficiency of plants, and thus reducing evapotranspiration and soil moisture losses. Several recent modeling studies suggest this effect could be quite important for projections of soil moisture and water resources (Cao et al, 2010; Wiltshire et al, 2013). We note, however, that empirical evidence for this water use efficiency effect as a large-scale control on the surface moisture balance is still highly uncertain. For example, Domec et al (2009) demonstrated for loblolly pine that the effect of enhanced [CO2] on stomatal conductance manifested only during times of high soil moisture, rather than drought. Naudts et al (2013), in a simulated drought experiment, found no significant ($p<0.10$) additional impact of elevated [CO2] on soil wetness, either before or after a drought manipulation (see their Figure 4, Table 1). Other experiments have found only modest changes ($< 15\%$) in evapotranspiration fluxes and soil water content with enhanced [CO2] (e.g., Hussain et al, 2013; Inauen et al, 2013; Stocker et al, 1997). Large uncertainties in the effect of enhanced [CO2] on future hydroclimate projections, namely through the modification of stomatal resistance, make characterizing the impact of this mechanism on a global scale simply too difficult to quantify for our purposes herein.

5 Conclusions.

This analysis provides a comprehensive accounting of how PET and precipitation changes will each affect global hydroclimate at the end of the 21^{st} century. For many regions, focusing on the precipitation response alone will be insufficient to fully capture changes in regional water resources such as soil moisture, runoff, or reservoir storage. Instead, increased evaporative demand will play a critical role in spreading drought beyond the sub-tropics and into the Northern Hemisphere mid-latitudes, regions of globally important agricultural production. China, for example, is the world's largest rice producer, a crop that serves as the primary nutrition source for more than 65% of the Chinese population (Peng et al, 2009). North America and much of central Asia are major centers of maize and wheat production; unlike China, they are also important exporters of these crops to the global marketplace (Headey, 2011). Increased temperatures, and the associated heat stresses, are already expected to negatively impact crop yields in these regions (Battisti and Naylor, 2009; Teixeira et al, 2013), and our analysis suggests that increases in PET due to warming and energy balance changes will have additional impacts through regional drying. Yield losses can be at least partially mitigated through management practices, such as modification of planting and harvest dates (Deryng et al, 2011). However, recent research suggests that climate change over the last 20 years is already having a deleterious impact on agricultural production (Lobell et al, 2011), and the ability of existing water resources to keep pace with future climate impacts is in question (Wada et al, 2013; Zhang et al, 2013). Even with pro-active management, our results suggest increased drying, driven primarily by increases in PET, will likely have significant ramifications for globally important regions of agricultural production in the Northern Hemisphere mid-latitudes.

Acknowledgements We acknowledge the World Climate Research Programme's Working Group on Coupled Modelling, which is responsible for CMIP, and we thank the climate modeling groups (listed in Table 1 of this paper) for producing and making available their model output. For CMIP, the U.S. Department of Energy's Program for Climate Model Diagnosis and Intercomparison provides coordinating support and led development of software infrastructure in partnership with the Global Organization for Earth System Science Portals. RS and JES were supported in part by the NOAA award Global Decadal Hydroclimate Variability and Change (NA10OAR431037). RS was also supported by NSF award ATM09-02716 and NOAA award NA08-OAR4320912. BIC was supported by NASA. LDEO Publication number #. We thank two anonymous reviewers for comments that greatly improved the quality of this manuscript.

References

Allen MR, Ingram WJ (2002) Constraints on future changes in climate and the hydrologic cycle. Nature 419(6903):224–232, DOI http://dx.doi.org/10.1038/nature01092

Allen RG, Pereira LS, Raes D, Smith M, et al (1998) Crop Evapotranspiration-Guidelines for Computing Crop Water Requirements. FAO Irrigation and Drainage Paper 56

Anderson DB (1936) Relative humidity or vapor pressure deficit. Ecology 17(2):277–282

Barnett TP, Pierce DW (2009) Sustainable water deliveries from the Colorado River in a changing climate. Proceedings of the National Academy of Sciences 106(18):7334–7338, DOI 10.1073/pnas.0812762106

Barrera-Escoda A, Gonçalves M, Guerreiro D, Cunillera J, Baldasano JM (2013) Projections of temperature and precipitation extremes in the North Western Mediterranean Basin by dynamical downscaling of climate scenarios at high resolution (1971–2050). Climatic Change pp 1–16, DOI 10.1007/s10584-013-1027-6

Battisti DS, Naylor RL (2009) Historical Warnings of Future Food Insecurity with Unprecedented Seasonal Heat. Science 323(5911):240–244, DOI 10.1126/science.1164363

Betts AK, Ball JH, Beljaars ACM, Miller MJ, Viterbo PA (1996) The land surface-atmosphere interaction: A review based on observational and global modeling perspectives. Journal of Geophysical Research: Atmospheres 101(D3):7209–7225, DOI 10.1029/95JD02135

Bonsal BR, Aider R, Gachon P, Lapp S (2013) An assessment of Canadian prairie drought: past, present, and future. Climate Dynamics 41(2):501–516, DOI 10.1007/s00382-012-1422-0

Burke EJ (2011) Understanding the Sensitivity of Different Drought Metrics to the Drivers of Drought under Increased Atmospheric CO2. Journal of Hydrometeorology 12(6):1378–1394, DOI 10.1175/2011JHM1386.1

Burke EJ, Brown SJ (2008) Evaluating Uncertainties in the Projection of Future Drought. Journal of Hydrometeorology 9(2):292–299, DOI 10.1175/2007JHM929.1

Burke EJ, Brown SJ, Christidis N (2006) Modeling the recent evolution of global drought and projections for the twenty-first century with the Hadley Centre climate model. Journal of Hydrometeorology 7(5):1113–1125, DOI http://dx.doi.org/10.1175/JHM544.1

Cao L, Bala G, Caldeira K, Nemani R, Ban-Weiss G (2010) Importance of carbon dioxide physiological forcing to future climate change. Proceedings of the National Academy of Sciences 107:9513—9518, DOI 10.1073/pnas.0913000107, http://www.pnas.org/content/early/2010/04/30/0913000107.full.pdf+html

Chou C, Neelin JD, Chen CA, Tu JY (2009) Evaluating the "Rich-Get-Richer"Mechanism in Tropical Precipitation Change under Global Warming. Journal of Climate 22(8):1982–2005, DOI 10.1175/2008JCLI2471.1

Chou C, Chiang JCH, Lan CW, Chung CH, Liao YC, Lee CJ (2013) Increase in the range between wet and dry season precipitation. Nature Geoscience 6(4):263–267, DOI http://dx.doi.org/10.1038/ngeo1744

Coats S, Smerdon JE, Seager R, Cook BI, González-Rouco JF (2013) Megadroughts in Southwestern North America in ECHO-G. Journal of Climate

e-View, DOI doi: 10.1175/JCLI-D-12-00603.1
Cook BI, Seager R, Miller RL, Mason JA (2013) Intensification of North American megadroughts through surface and dust aerosol forcing. Journal of Climate 26:4414–4430, DOI http://dx.doi.org/10.1175/JCLI-D-12-00022.1
Cook ER, Seager R, Heim Jr RR, Vose RS, Herweijer C, Woodhouse C (2010) Megadroughts in North America: placing IPCC projections of hydroclimatic change in a long-term palaeoclimate context. Journal of Quaternary Science 25(1):48–61, DOI 10.1002/jqs.1303
Coumou D, Rahmstorf S (2012) A decade of weather extremes. Nature Climate Change 2(7):491–496, DOI 10.1038/nclimate1452
Dai A (2011a) Characteristics and trends in various forms of the Palmer Drought Severity Index during 1900–2008. Journal of Geophysical Research: Atmospheres 116(D12):D12,115, DOI 10.1029/2010JD015541
Dai A (2011b) Drought under global warming: a review. Wiley Interdisciplinary Reviews: Climate Change 2(1):45–65, DOI 10.1002/wcc.81
Dai A (2013) Increasing drought under global warming in observations and models. Nature Climate Change 3(1):52–58, DOI 10.1038/nclimate1633
Deryng D, Sacks WJ, Barford CC, Ramankutty N (2011) Simulating the effects of climate and agricultural management practices on global crop yield. Global Biogeochemical Cycles 25(2), DOI 10.1029/2009GB003765
Ding Y, Hayes MJ, Widhalm M (2011) Measuring economic impacts of drought: a review and discussion. Disaster Prevention and Management 20(4):434–446, DOI 10.1108/09653561111161752
Domec JC, Palmroth S, Ward E, Maier CA, Thérézien M, Oren R (2009) Acclimation of leaf hydraulic conductance and stomatal conductance of Pinus taeda (loblolly pine) to long-term growth in elevated CO2 (free-air CO2 enrichment) and N-fertilization. Plant, Cell & Environment 32(11):1500–1512, DOI 10.1111/j.1365-3040.2009.02014.x
Giannini A, Saravanan R, Chang P (2003) Oceanic Forcing of Sahel Rainfall on Interannual to Interdecadal Time Scales. Science 302(5647):1027–1030, DOI 10.1126/science.1089357
Guttman NB (1998) Comparing the Palmer Drought Index and the Standardized Precipitation Index. Journal of the American Water Resources Association 34:113–121, DOI 10.1111/j.1752-1688.1998.tb05964.x
Headey D (2011) Rethinking the global food crisis: The role of trade shocks. Food Policy 36(2):136 – 146, DOI http://dx.doi.org/10.1016/j.foodpol.2010.10.003
Held I, Soden B (2006) Robust responses of the hydrological cycle to global warming. Journal of Climate 19(21):5686–5699, DOI http://dx.doi.org/10.1175/JCLI3990.1
Hernandez E, Uddameri V (2013) Standardized precipitation evaporation index (SPEI)-based drought assessment in semi-arid south Texas. Environmental Earth Sciences pp 1–11, DOI 10.1007/s12665-013-2897-7
Hoerling M, Kumar A, Dole R, Nielsen-Gammon JW, Eischeid J, Perlwitz J, Quan XW, Zhang T, Pegion P, Chen M (2012a) Anatomy of an Extreme Event. Journal of Climate 26(9):2811–2832, DOI 10.1175/JCLI-D-12-00270.1
Hoerling M, Eischeid J, Kumar A, Leung R, Mariotti A, Mo K, Schubert S, Seager R (2013) Causes and Predictability of the 2012 Great Plains Drought. Bulletin of the American Meteorological Society in press

Hoerling MP, Eischeid JK, Quan XW, Diaz HF, Webb RS, Dole RM, Easterling DR (2012b) Is a Transition to Semipermanent Drought Conditions Imminent in the U.S. Great Plains? Journal of Climate 25(24):8380–8386, DOI 10.1175/JCLI-D-12-00449.1

Huntington TG (2006) Evidence for intensification of the global water cycle: Review and synthesis. Journal of Hydrology 319(1–4):83–95, DOI http://dx.doi.org/10.1016/j.jhydrol.2005.07.003

Hussain MZ, VanLoocke A, Siebers MH, Ruiz-Vera UM, Cody Markelz RJ, Leakey ADB, Ort DR, Bernacchi CJ (2013) Future carbon dioxide concentration decreases canopy evapotranspiration and soil water depletion by field-grown maize. Global Change Biology 19(5):1572–1584, DOI 10.1111/gcb.12155

Inauen N, Körner C, Hiltbrunner E (2013) Hydrological consequences of declining land use and elevated CO2 in alpine grassland. Journal of Ecology 101(1):86–96, DOI 10.1111/1365-2745.12029, URL http://dx.doi.org/10.1111/1365-2745.12029

Jung M, Reichstein M, Ciais P, Seneviratne SI, Sheffield J, Goulden ML, Bonan G, Cescatti A, Chen J, de Jeu R, Dolman AJ, Eugster W, Gerten D, Gianelle D, Gobron N, Heinke J, Kimball J, Law BE, Montagnani L, Mu Q, Mueller B, Oleson K, Papale D, Richardson AD, Roupsard O, Running S, Tomelleri E, Viovy N, Weber U, Williams C, Wood E, Zaehle S, Zhang K (2010) Recent decline in the global land evapotranspiration trend due to limited moisture supply. Nature 467(7318):951–954, DOI http://dx.doi.org/10.1038/nature09396

Karl TR, Gleason BE, Menne MJ, McMahon JR, Heim RR, Brewer MJ, Kunkel KE, Arndt DS, Privette JL, Bates JJ, Groisman PY, Easterling DR (2012) U.S. temperature and drought: Recent anomalies and trends. EOS, Transactions of the American Geophysical Union 93(47):473–474, DOI 10.1029/2012EO470001

Knutti R, Sedlacek J (2013) Robustness and uncertainties in the new CMIP5 climate model projections. Nature Climate Change 3(4):369–373, DOI 10.1038/nclimate1716

Lee JY, Wang B (2012) Future change of global monsoon in the CMIP5. Climate Dynamics pp 1–19, DOI 10.1007/s00382-012-1564-0

Li X, Waddington SR, Dixon J, Joshi AK, Vicente MC (2011) The relative importance of drought and other water-related constraints for major food crops in South Asian farming systems. Food Security 3(1):19–33, DOI 10.1007/s12571-011-0111-x

Lobell DB, Schlenker W, Costa-Roberts J (2011) Climate Trends and Global Crop Production Since 1980. Science 333(6042):616–620, DOI 10.1126/science.1204531

Lubchenco J, Karl TR (2012) Predicting and managing extreme weather events. Physics Today 65(3):31, DOI http://dx.doi.org/10.1063/PT.3.1475

Lyon B, DeWitt DG (2012) A recent and abrupt decline in the East African long rains. Geophysical Research Letters 39(2):L02,702, DOI 10.1029/2011GL050337

McGrath GS, Sadler R, Fleming K, Tregoning P, Hinz C, Veneklaas EJ (2012) Tropical cyclones and the ecohydrology of Australia's recent continental-scale drought. Geophysical Research Letters 39(3), DOI 10.1029/2011GL050263

McKee TB, Doesken NJ, Kleist J (1993) The relationship of drought frequency and duration to time scales. Eighth Conference on Applied Climatology pp 179–184

Meehl GA, Zwiers F, Evans J, Knutson T, Mearns L, Whetton P (2000) Trends in Extreme Weather and Climate Events: Issues Related to Mod-

eling Extremes in Projections of Future Climate Change*. Bulletin of the American Meteorological Society 81(3):427–436, DOI 10.1175/1520-0477(2000)081¡0427:TIEWAC¿2.3.CO;2
Naudts K, Berge J, Janssens I, Nijs I, Ceulemans R (2013) Combined effects of warming and elevated CO2 on the impact of drought in grassland species. Plant and Soil 369(1-2):497–507, DOI 10.1007/s11104-013-1595-2
Neelin JD, Chou C, Su H (2003) Tropical drought regions in global warming and El Nino teleconnections. Geophysical Research Letters 30(24), DOI 10.1029/2003GL018625
Palmer WC (1965) Meteorological drought. Research paper 45:1–58
Peng S, Tang Q, Zou Y (2009) Current Status and Challenges of Rice Production in China. Plant Production Science 12(1):3–8, DOI http://dx.doi.org/10.1626/pps.12.3
Penman HL (1948) Natural Evaporation from Open Water, Bare Soil and Grass. Proceedings of the Royal Society of London Series A Mathematical and Physical Sciences 193(1032):120–145
Rahmstorf S, Coumou D (2011) Increase of extreme events in a warming world. Proceedings of the National Academy of Sciences 108(44):17,905–17,909, DOI 10.1073/pnas.1101766108
Rosenzweig C, Hillel D (1993) The dust bowl of the 1930s: Analog of greenhouse effect in the Great Plains? Journal of Environmental Quality 22(1):9–22
Ross TF, Lott N (2003) A climatology of 1980-2003 extreme weather and climate events. Tech. rep., NOAA/NESDIS. National Climatic Data Center, Asheville, NC.
Scheff J, Frierson DMW (2013) Scaling Potential Evapotranspiration with Greenhouse Warming. Journal of Climate DOI 10.1175/JCLI-D-13-00233.1
van der Schrier G, Barichivich J, Briffa KR, Jones PD (2013) A scPDSI-based global data set of dry and wet spells for 1901–2009. Journal of Geophysical Research: Atmospheres DOI 10.1002/jgrd.50355
Seager R, Burgman R, Kushnir Y, Clement A, Cook E, Naik N, Miller J (2008) Tropical Pacific forcing of North American Medieval Megadroughts: Testing the Concept with an Atmosphere Model Forced by Coral-Reconstructed SSTs. Journal of Climate 21(23):6175–6190, DOI http://dx.doi.org/10.1175/2008JCLI2170.1
Seager R, Naik N, Vecchi GA (2010) Thermodynamic and Dynamic Mechanisms for Large-Scale Changes in the Hydrological Cycle in Response to Global Warming. Journal of Climate 23(17):4651–4668, DOI 10.1175/2010JCLI3655.1
Seager R, Ting M, Li C, Naik N, Cook B, Nakamura J, Liu H (2013) Projections of declining surface-water availability for the southwestern United States. Nature Climate Change 3:482–486, DOI 10.1038/nclimate1787
Sellers PJ, Dickinson RE, Randall DA, Betts AK, Hall FG, Berry JA, Collatz GJ, Denning AS, Mooney HA, Nobre CA, Sato N, Field CB, Henderson-Sellers A (1997) Modeling the Exchanges of Energy, Water, and Carbon Between Continents and the Atmosphere. Science 275(5299):502–509, DOI 10.1126/science.275.5299.502
Seneviratne SI (2012) Climate science: Historical drought trends revisited. Nature 491(7424):338–339, URL http://dx.doi.org/10.1038/491338a
Seo KH, Ok J, Son JH, Cha DH (2013) Assessing future changes in the East Asian summer monsoon using CMIP5 coupled models. Journal of Climate DOI

10.1175/JCLI-D-12-00694.1
Sheffield J, Wood EF (2008) Projected changes in drought occurrence under future global warming from multi-model, multi-scenario, IPCC AR4 simulations. Climate Dynamics 31(1):79–105, DOI 10.1007/s00382-007-0340-z
Sheffield J, Wood EF, Roderick ML (2012) Little change in global drought over the past 60 years. Nature 491(7424):435–438, DOI 10.1038/nature11575
Stocker R, Leadley PW, Körner C (1997) Carbon and water fluxes in a calcareous grassland under elevated CO2. Functional Ecology 11(2):222–230, DOI 10.1046/j.1365-2435.1997.00071.x
Taylor IH, Burke E, McColl L, Falloon PD, Harris GR, McNeall D (2013) The impact of climate mitigation on projections of future drought. Hydrology and Earth System Sciences 17(6):2339–2358, DOI 10.5194/hess-17-2339-2013
Taylor KE, Stouffer RJ, Meehl GA (2012) An Overview Of CMIP5 And The Experiment Design. Bulletin of the American Meteorological Society 93(4):485–498, DOI http://dx.doi.org/10.1175/BAMS-D-11-00094.1
Teixeira EI, Fischer G, van Velthuizen H, Walter C, Ewert F (2013) Global hot-spots of heat stress on agricultural crops due to climate change. Agricultural and Forest Meteorology 170(0):206—215, DOI http://dx.doi.org/10.1016/j.agrformet.2011.09.002
Thornthwaite C (1948) An approach toward a rational classification of climate. Geographical review 38(1):55–94
Vicente-Serrano SM, Beguería S, López-Moreno JI (2009) A Multiscalar Drought Index Sensitive to Global Warming: The Standardized Precipitation Evapotranspiration Index. Journal of Climate 23(7):1696–1718, DOI 10.1175/2009JCLI2909.1
Vicente-Serrano SM, Beguería S, López-Moreno JI, Angulo M, El Kenawy A (2010) A new global 0.5 gridded dataset (1901-2006) of a multiscalar drought index: comparison with current drought index datasets based on the Palmer Drought Severity Index. Journal of Hydrometeorology 11(4):1033–1043, DOI http://dx.doi.org/10.1175/2010JHM1224.1
Wada Y, Wisser D, Eisner S, Flörke M, Gerten D, Haddeland I, Hanasaki N, Masaki Y, Portmann FT, Stacke T, Tessler Z, Schewe J (2013) Multi-model projections and uncertainties of irrigation water demand under climate change. Geophysical Research Letters DOI 10.1002/grl.50686
Wiltshire A, Gornall J, Booth B, Dennis E, Falloon P, Kay G, McNeall D, McSweeney C, Betts R (2013) The importance of population, climate change and {CO2} plant physiological forcing in determining future global water stress. Global Environmental Change 23(5):1083 – 1097, DOI http://dx.doi.org/10.1016/j.gloenvcha.2013.06.005
Xu CY, Singh VP (2002) Cross Comparison of Empirical Equations for Calculating Potential Evapotranspiration with Data from Switzerland. Water Resources Management 16(3):197–219, DOI 10.1023/A:1020282515975
Zhang T, Simelton E, Huang Y, Shi Y (2013) A Bayesian assessment of the current irrigation water supplies capacity under projected droughts for the 2030s in China. Agricultural and Forest Meteorology 178–179(0):56 – 65, DOI dx.doi.org/10.1016/j.agrformet.2012.06.002

Table 1 Continuous model ensembles from the CMIP5 experiments (historical+RCP8.5) used in this analysis, including the modeling center or group that supplied the output, the number of ensemble members that met our criteria for inclusion, and the approximate spatial resolution.

Model	Modeling Center (or Group)	# Runs	Lat/Lon Resolution
CanESM2	CCCMA[a]	5	2.8°x2.8°
CCSM4	NCAR[b]	6	0.94°x1.25°
CNRM-CM5	CNRM-CERFACS[c]	4	1.4°x1.4°
CSIRO-MK3.6.0	CSIRO-QCCCE[d]	5	1.87°x1.87°
GFDL-CM3	NOAA GFDL[e]	1	2.0°x2.5°
GFDL-ESM2G	NOAA GFDL[e]	1	2.0°x2.5°
GFDL-ESM2M	NOAA GFDL[e]	1	2.0°x2.5°
GISS-E2-R	NASA GISS[f]	1	2.0°x2.5°
INMCM4.0	INM[g]	1	1.5°x2.0°
IPSL-CM5A-LR	IPSL[h]	4	1.9°x3.75°
MIROC5	MIROC[i]	1	1.4°x1.4°
MIROC-ESM	MIROC[j]	1	2.8°x2.8°
MIROC-ESM-CHEM	MIROC[j]	1	2.8°x2.8°
MRI-CGCM3	MRI[k]	1	1.1°x1.1°
NorESM1-M	NCC[l]	1	1.9°x2.5°

[a]Canadian Centre for Climate Modelling and Analysis
[b]National Center for Atmospheric Research
[c]Centre National de Recherches Météorologiques / Centre Européen de Recherche et Formation Avancée en Calcul Scientifique
[d]Commonwealth Scientific and Industrial Research Organization in collaboration with Queensland Climate Change Centre of Excellence
[e]NOAA Geophysical Fluid Dynamics Laboratory
[f]NASA Goddard Institute for Space Studies
[g]Institute for Numerical Mathematics
[h]Institut Pierre-Simon Laplace
[i]Atmosphere and Ocean Research Institute (The University of Tokyo), National Institute for Environmental Studies, and Japan Agency for Marine-Earth Science and Technology
[j]Japan Agency for Marine-Earth Science and Technology, Atmosphere and Ocean Research Institute (The University of Tokyo), and National Institute for Environmental Studies
[k]Meteorological Research Institute
[l]Norwegian Climate Centre

Table 2 Description of different versions of the PDSI and SPEI calculations, and the model diagnostics used in their calculation. Variables are: tsurf (2-meter surface air temperature), prec (precipitation), q (specific humidity), and rnet (surface net radiation). Detrended variables have the trend from 2000–2099 removed and replaced with mean conditions for 1980–1999.

PDSI/SPEI	Transient Variables	Detrended Variables
PDSI-ALL, SPEI-ALL	tsurf, prec, q, rnet	none
PDSI-PRE, SPEI-PRE	prec	tsurf, q, rnet
PDSI-PET, SPEI-PET	tsurf, q, rnet	prec

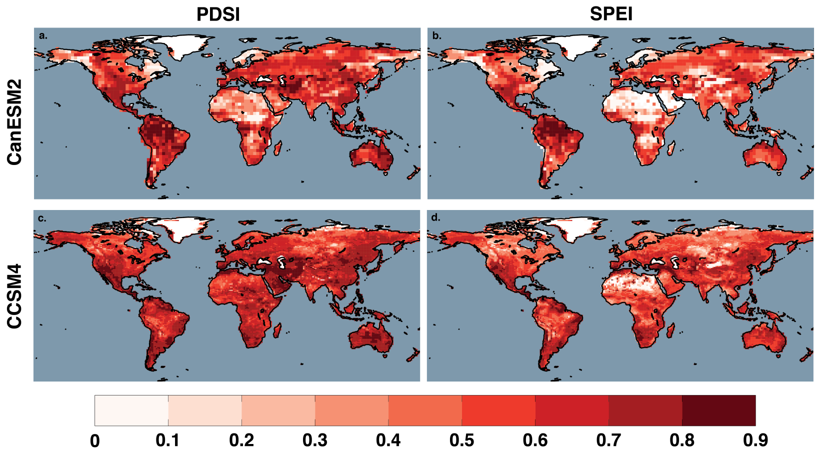

Fig. 1 Pearson's correlation coefficients calculated between PDSI (a,c) and SPEI (b,d) and annual average model soil moisture from the approximate top 30 centimeters of the soil column: CanESM2 (a,b) and CCSM4 (c,d). Maps represent average correlations across a five member ensemble for each model; the comparison interval is 1901-2099.

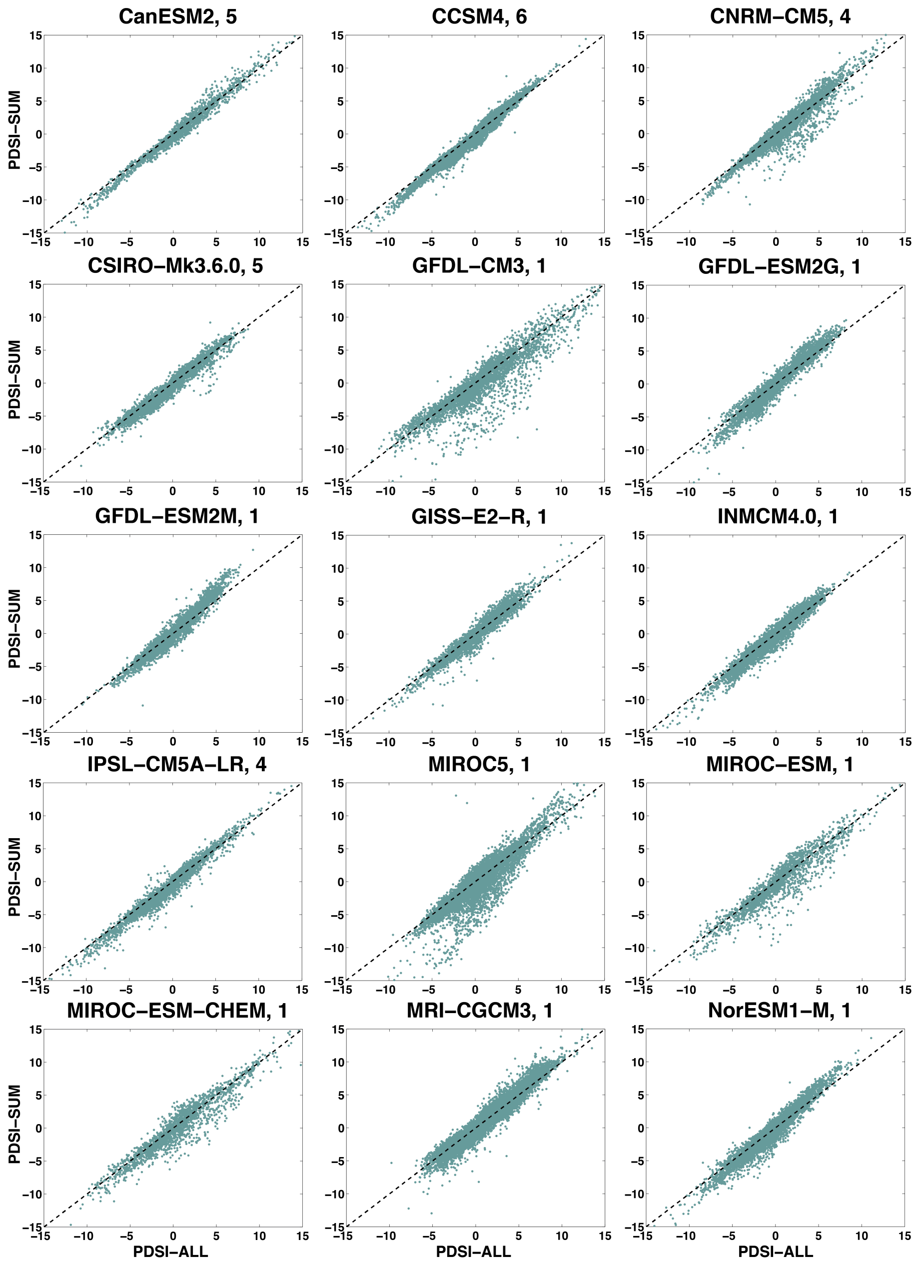

Fig. 2 Grid cell comparisons between ensemble averaged annual PDSI (PDSI-ALL) and PDSI-SUM (PDSI-PRE + PDSI-ET) from 2080-2099 for each model in the ensemble. The dashed line indicates the 1:1 line. For those models with multiple ensemble members, the comparison is based on the ensemble average. PDSI-SUM scales linearly with PDSI-ALL, close to the 1:1 line, with some minor amplification of extreme wet or dry values in PDSI-SUM. This suggests that PDSI-ALL is well approximated as a linear sum of the pseudo-independent effects of precipitation and evapotranspiration.

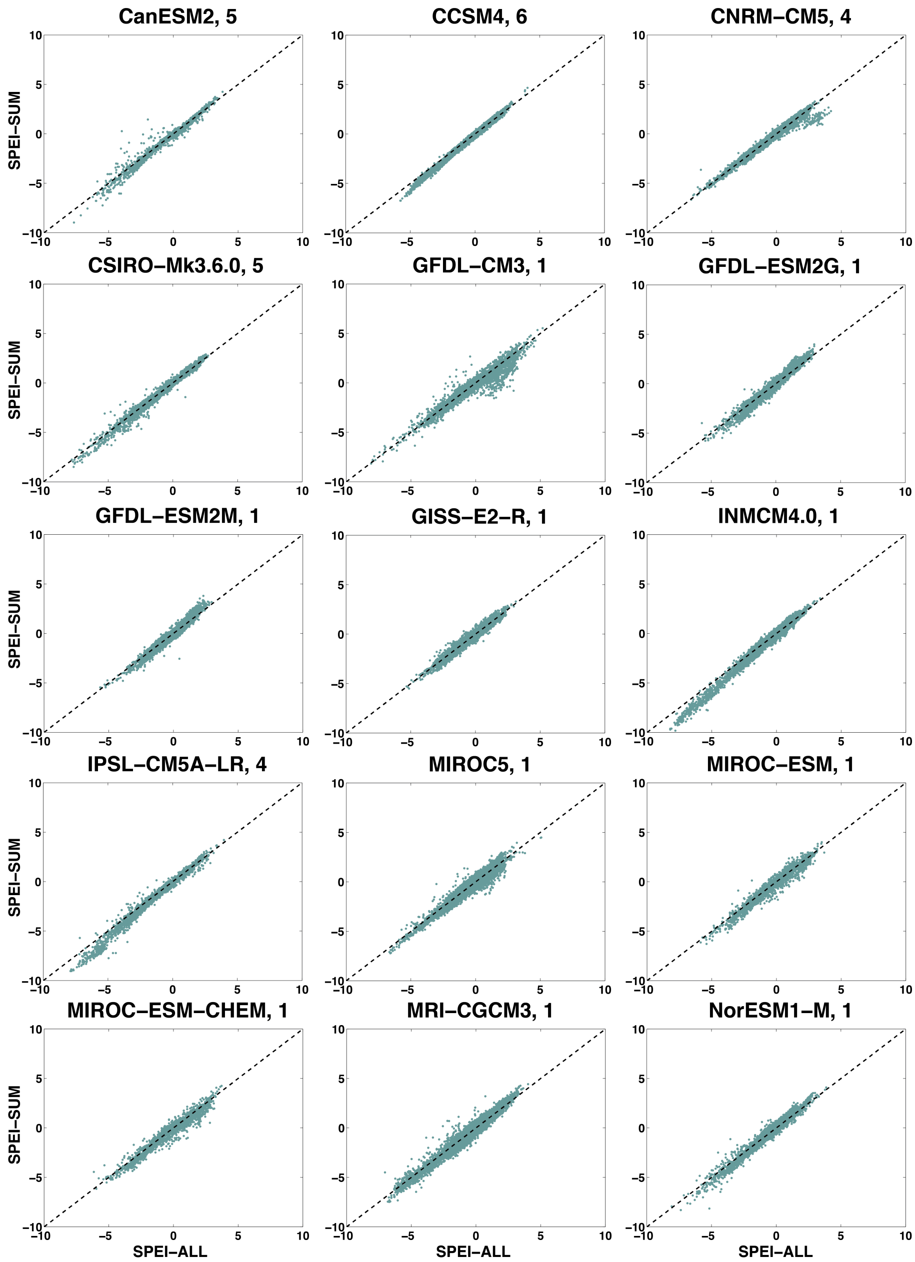

Fig. 3 Same as Figure 2, but for the 12-month SPEI-ALL and SPEI-SUM calculations.

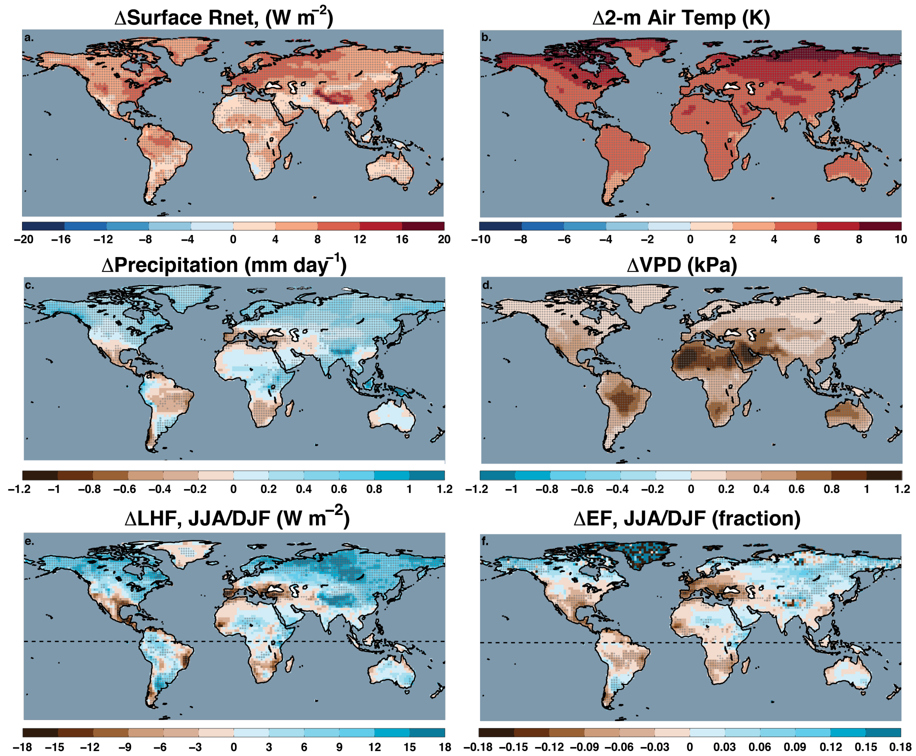

Fig. 4 Multi-model mean changes (2080–2099 minus 1931–1990) in a) surface net radiation (W m^{-2}), b) 2-meter air temperature (K), c) precipitation (mm day^{-1}), d) vapor pressure deficit (kPa), e) latent heat fluxes (W m^{-2}), and f) evaporative fraction (fraction). Panels a)–d) are annual averages. In e)–f), averages north of the equator (the dashed line) are for boreal summer (June–July–August) and south of the equator are for austral summer (December–January–February). Cross hatching indicates areas where the sign of the change in at least 12 of the 15 models agrees with the sign of the multi-model mean.

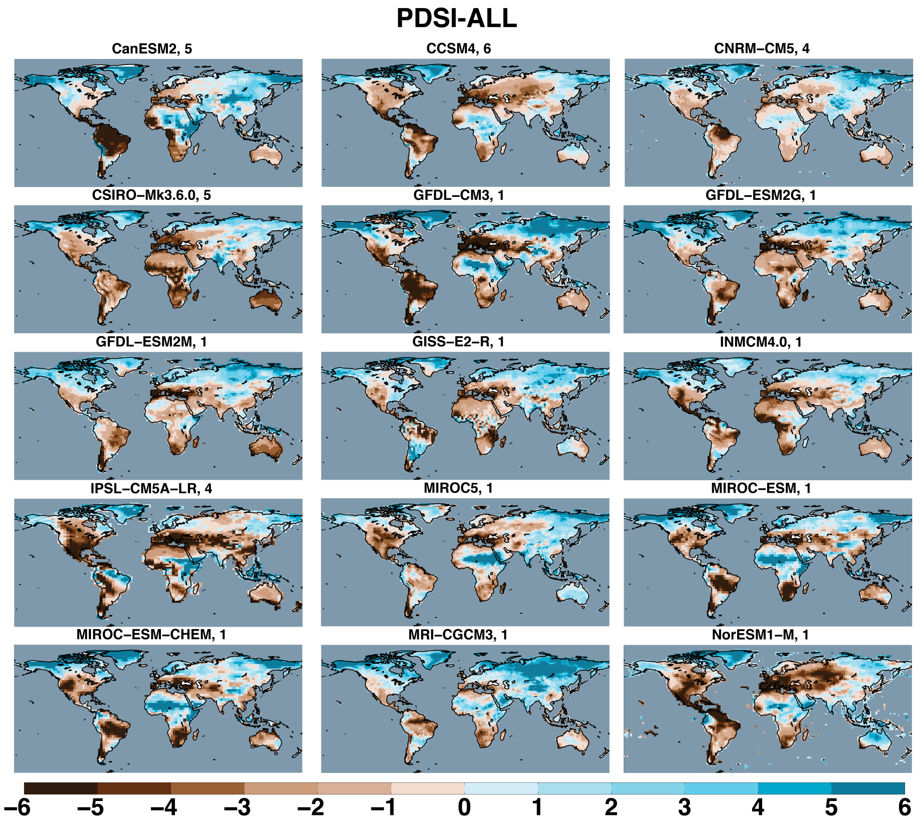

Fig. 5 Annual averaged PDSI-ALL from 2080–2099 for each model simulation under the RCP8.5 scenario. The number of ensemble members is listed in each panel title; for models with multiple ensemble members, the maps represent the ensemble average.

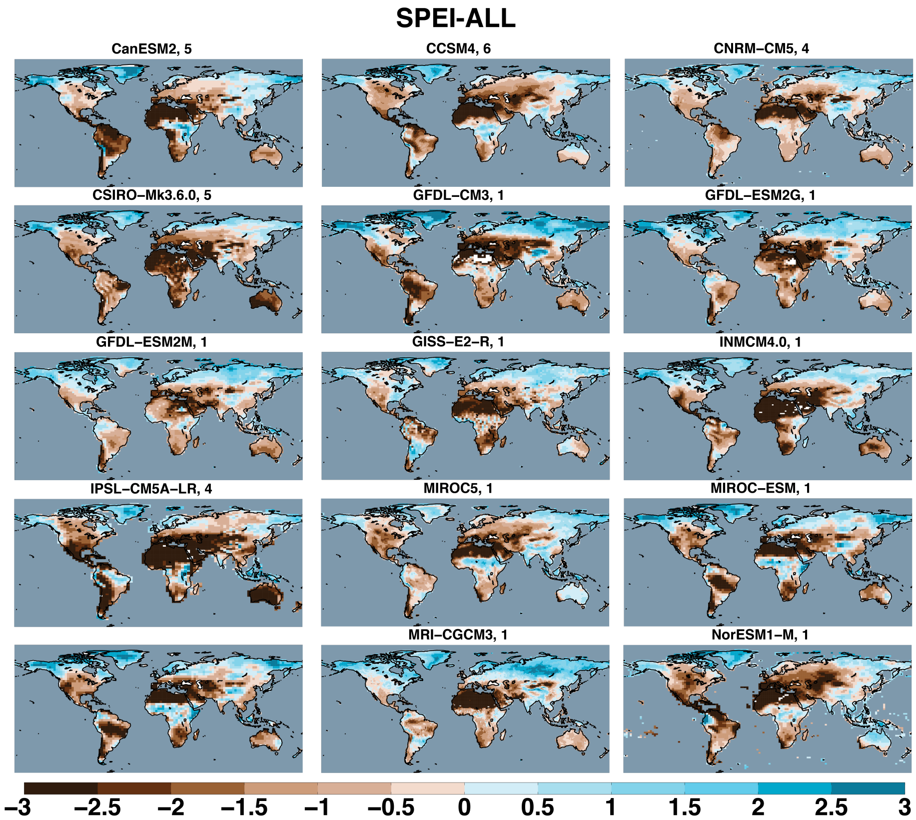

Fig. 6 Same as Figure 5, but for SPEI-ALL.

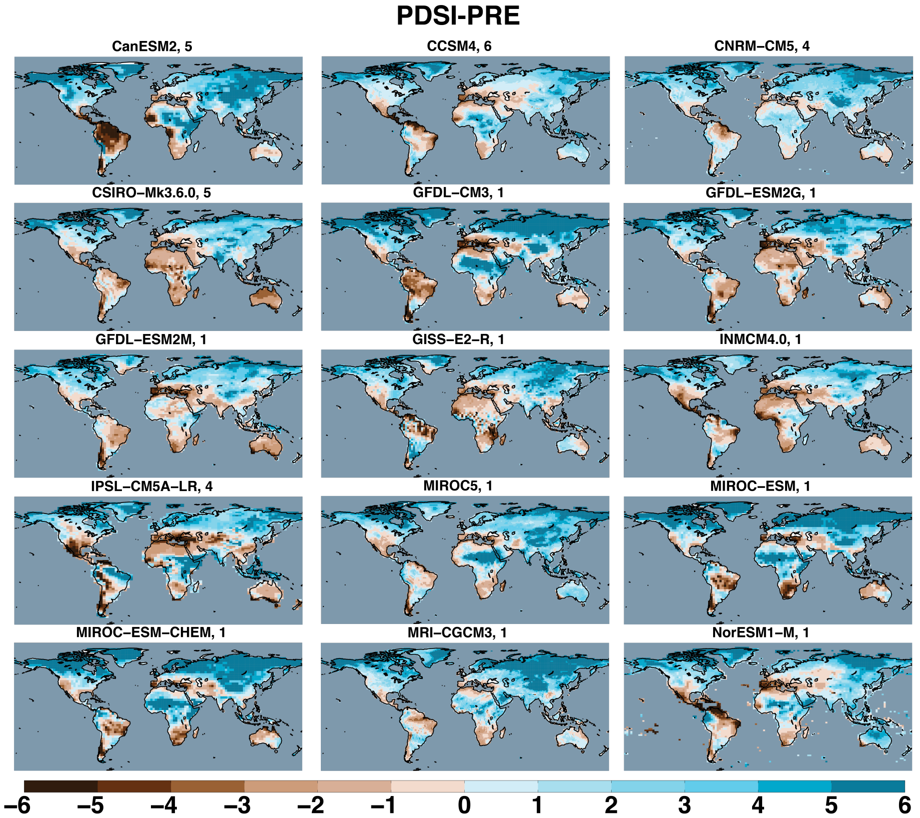

Fig. 7 Annual averaged PDSI-PRE (precipitation effects only) for each model simulation under the RCP8.5 scenario. The number of ensemble members is listed in each panel title; for models with multiple ensemble members, the maps represent the ensemble average.

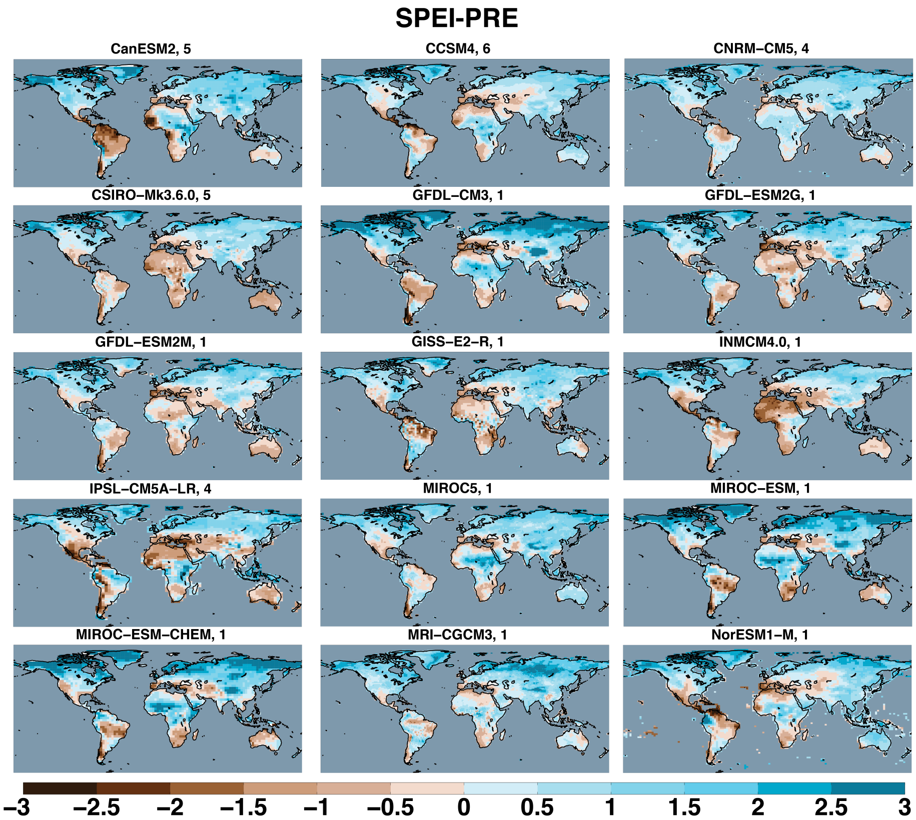

Fig. 8 Same as Figure 7, but for SPEI-PRE.

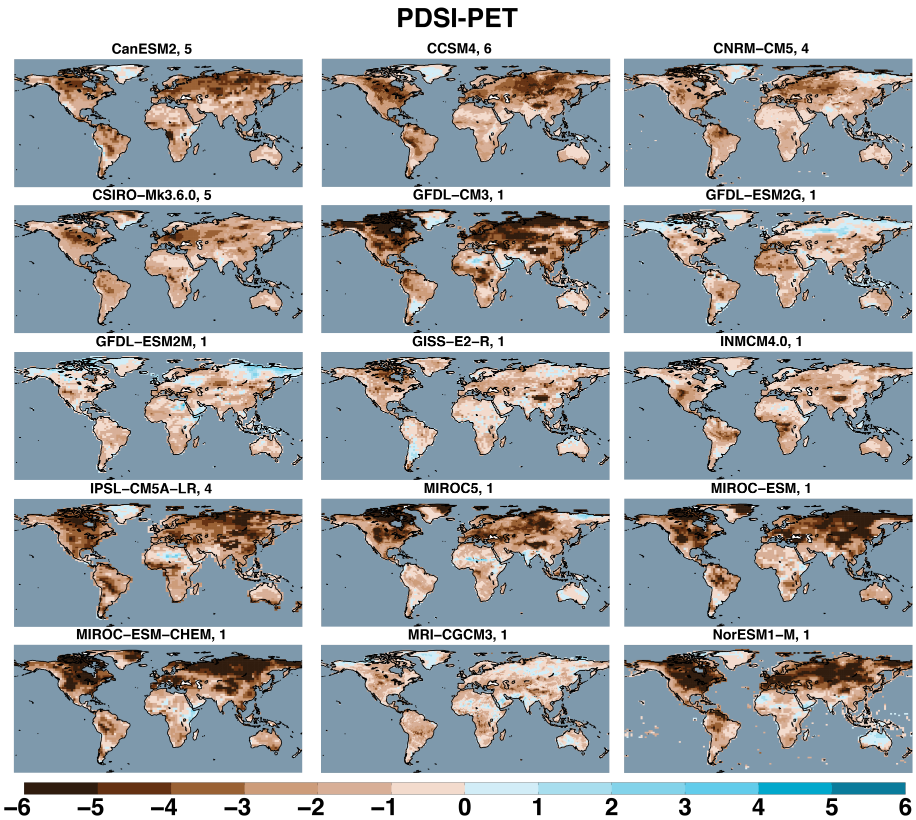

Fig. 9 Annual averaged PDSI-PET (evaporative demand effects only) for each model simulation under the RCP8.5 scenario. The number of ensemble members is listed in each panel title; for models with multiple ensemble members, the maps represent the ensemble average.

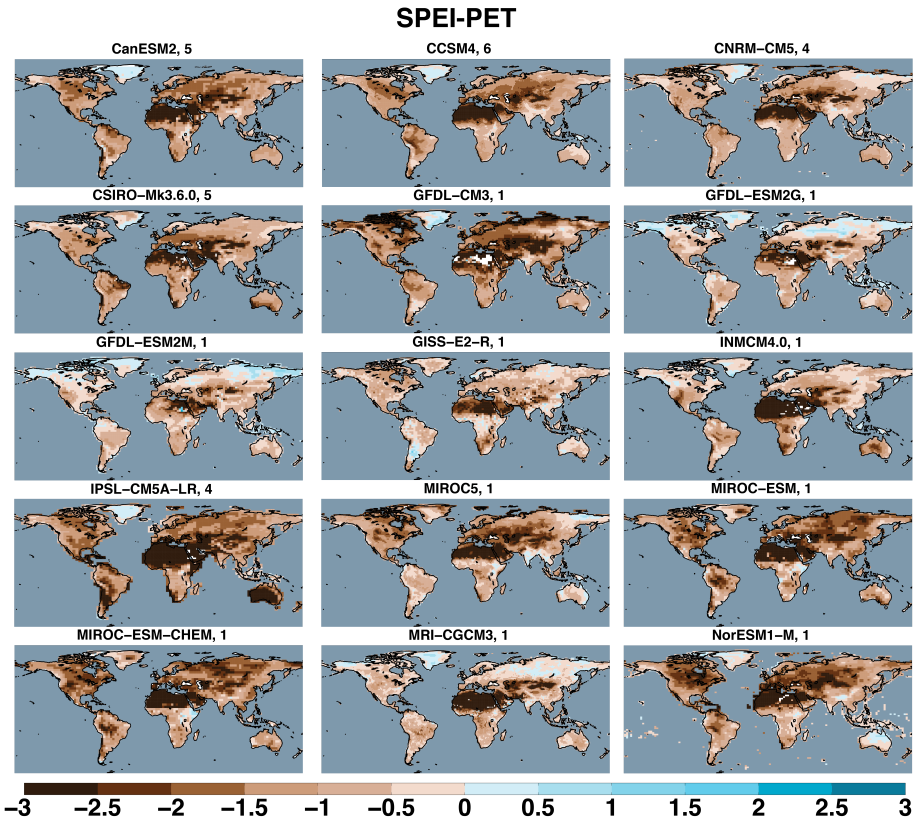

Fig. 10 Same as Figure 9, but for SPEI-PET.

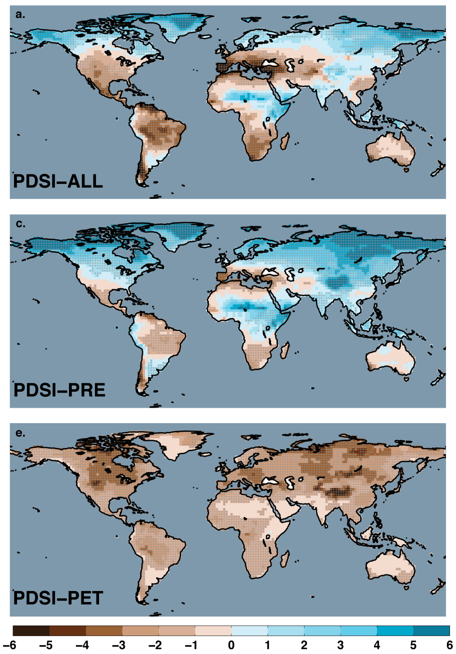

Fig. 11 Multi-model mean PDSI-ALL (a), SPEI-ALL (b), PDSI-PRE (c), SPEI-PRE (d), PDSI-PET (e), and SPEI-PET (f) for 2080-2099. For PDSI, cross-hatching indicates cells where, for multi-model mean PDSI anomalies exceeding -1 or +1, at least 12 of the 15 models (80%) also exceed these thresholds. For SPEI, the cross-hatching threshold is for 80% agreement with threshold values of -0.5 or +0.5 in the multi-model mean.

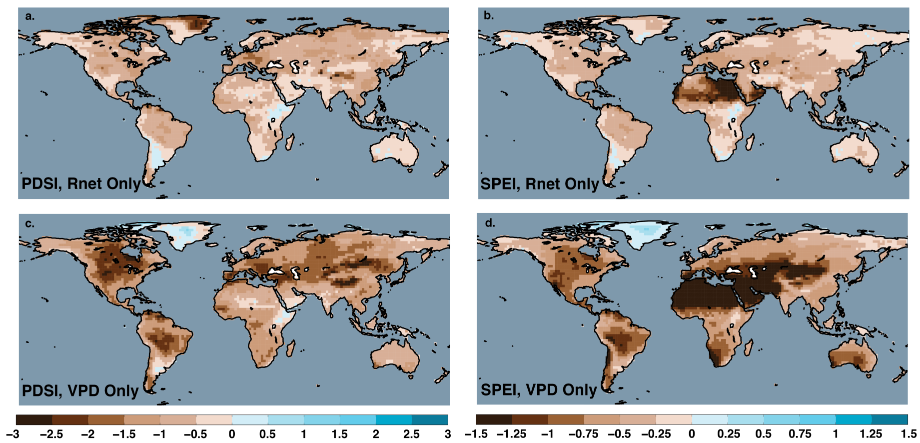

Fig. 12 Multi-model mean PDSI (a,c) and SPEI (b,d) projections for 2080-2090, incorporating only trends in a) surface net radiation and b) vapor pressure deficit. Note the range of values on the colorbars are half that of the other PDSI and SPEI maps, in order to better illustrate the changes.

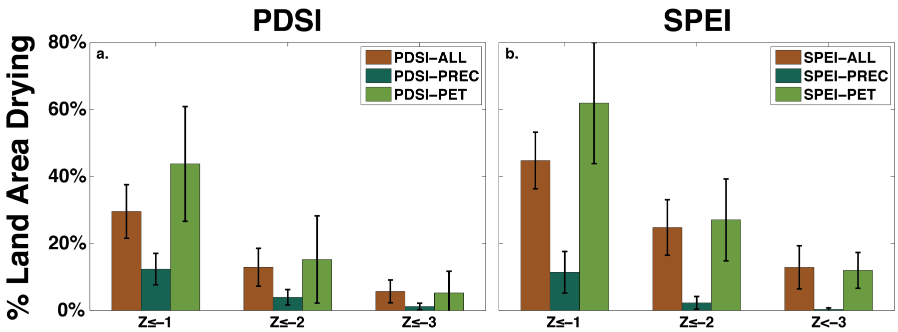

Fig. 13 Percent land area (excluding Antarctica) with annual average 2080–2099 PDSI (a) and SPEI (b) exceeding 1, 2, or 3 standard deviations. Bars represent the multi-model mean, and the error bars are the +/-1 standard deviation calculated across models. For models with multiple ensemble members, the ensemble average is calculated first and then used for the multi-model statistics.

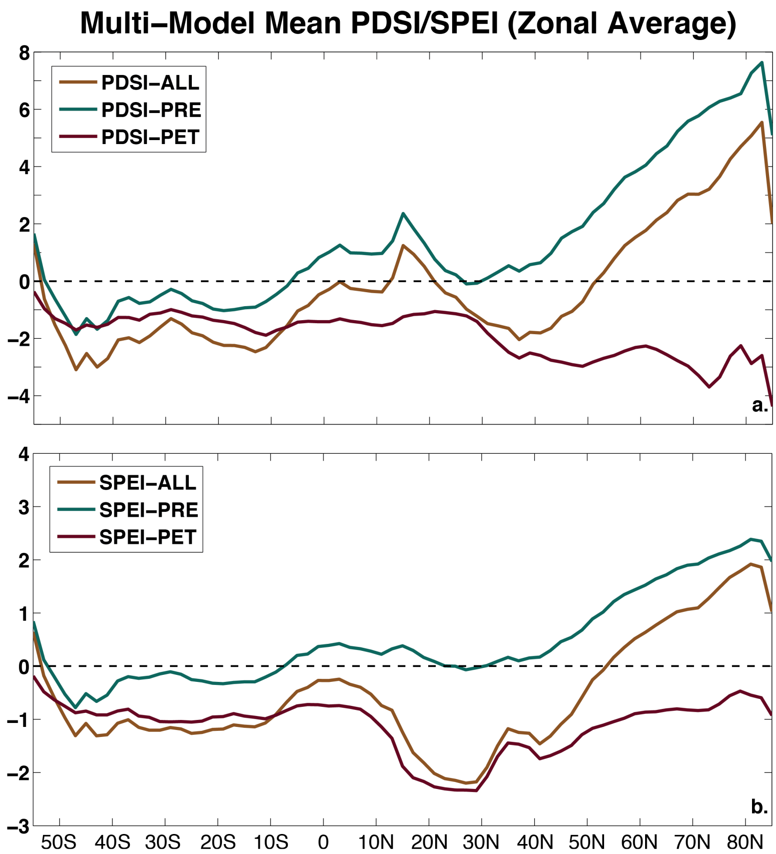

Fig. 14 Zonally averaged multi-model mean PDSI (a) and SPEI (b) from 2080-2099.

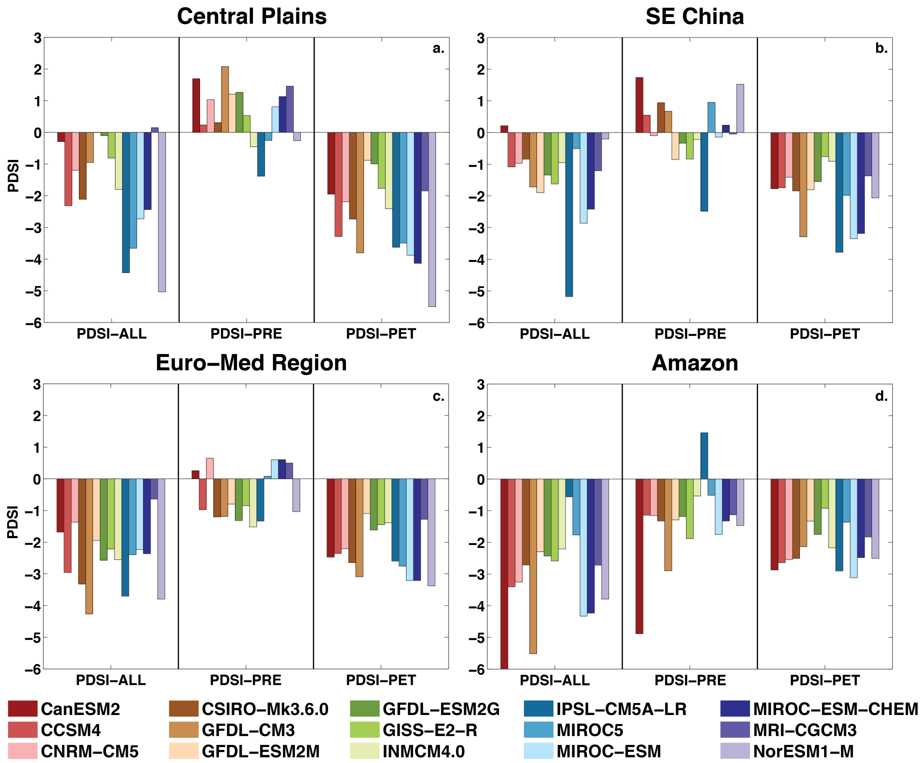

Fig. 15 Regionally averaged PDSI for each model, over a) the Central Plains of North America (105°W-90°W, 32°N-50°N), b) southeast China (102°E-123°E, 22°N-30°N), c) the European-Mediterranean region (20°W-50°E, 28°N-60°N), and d) the Amazon (70°W-45°W, 20°S-5°N).

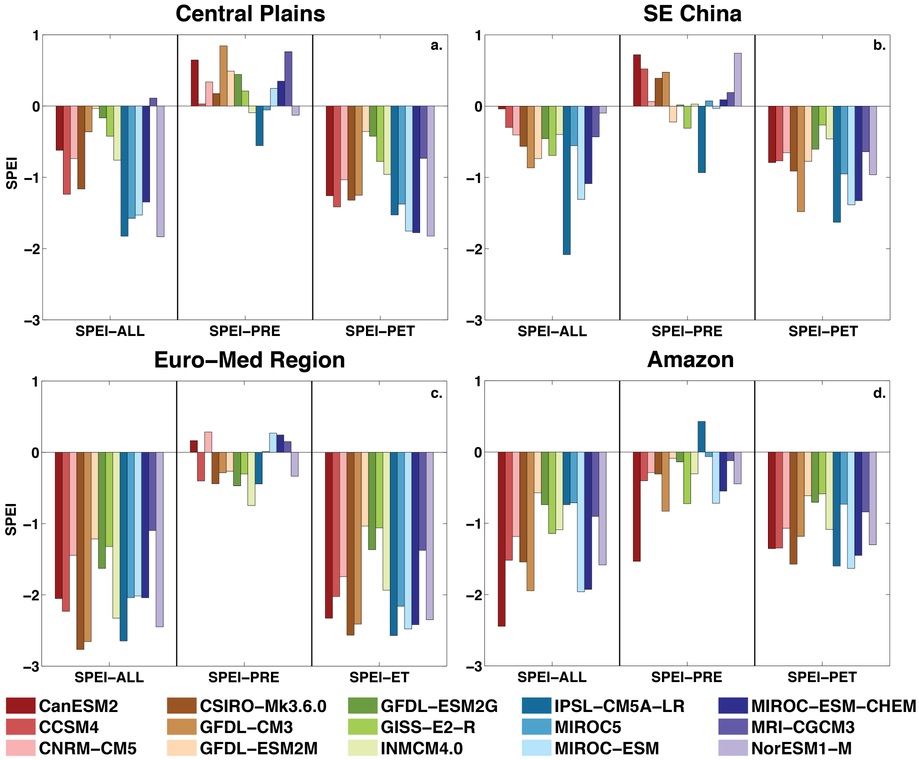

Fig. 16 Same as Figure 15, but for SPEI.